

A closer look at a hint of SUSY at the 8 TeV LHC

Philipp Grothaus^(a,1), Seng Pei Liew^(b,2) and Kazuki Sakurai^(a,3)

^a*Department of Physics, King's College London, London WC2R 2LS, UK*

^b*Department of Physics, University of Tokyo, Bunkyo-ku, Tokyo 113-0033, Japan*

Abstract

A recent CMS analysis has reported the observation of an excess in the invariant mass distribution of the opposite-sign same-flavour lepton pair, which can be interpreted as a kinematic edge due to new physics. Using collider simulation tools, we recast relevant LHC search results reported by ATLAS and CMS collaborations in order to determine constraints on supersymmetric models that could produce the observed features. In particular, we focus on models involving cascade decays of light-flavour squarks and sbottoms. We find no favourable supersymmetry scenario within our exploration that could explain the origin of the excess when other LHC constraints are taken into account.

¹philipp.grothaus@kcl.ac.uk

²liew@hep-th.phys.s.u-tokyo.ac.jp

³kazuki.sakurai@kcl.ac.uk

1 Introduction

The search for supersymmetry (SUSY) as an extension of the Standard Model (SM) is one major target of the Large Hadron Collider (LHC) physics program. However, we have thus far found no definitive evidence of SUSY based on the first run of the LHC despite dedicated searches on many fronts. Even so, there is an analysis presented by the CMS collaboration that could be showing the first signs of SUSY [1, 2]. In the analysis, two leptons, jets and missing energy are looked for in the final states. It is found that there is an excess (130_{-49}^{+48} events in the “central” region) in the invariant mass distribution of the opposite-sign same-flavour (OSSF) lepton pair, corresponding to a significance of 2.6σ .

The excess of the signal is fitted kinematically as a triangular-shape edge at $m_{\ell\ell} = 78.7 \pm 1.4$ GeV. Such a kinematic edge is a characteristic signal of SUSY, where a SUSY particle undergoes a two-stage two-body decay. The kinematic edge formed by a pair of leptons can be interpreted as the cascade decay of a neutralino: $\tilde{\chi}_2^0 \rightarrow \tilde{\ell}^\pm \ell^\mp \rightarrow \ell^\pm \ell^\mp \tilde{\chi}_1^0$ (on-shell slepton decay) [3]. It is also possible to interpret the edge as a three-body decay signal of a neutralino, $\tilde{\chi}_2^0 \rightarrow \ell^\pm \ell^\mp \tilde{\chi}_1^0$, where the lepton pair is produced via an off-shell Z (off-shell Z decay). The shape of the edge would be more rounded as compared to the two-stage two-body decay, but as shown in the original CMS analysis, the three-body decay still provides a good fit. The direct production of $\tilde{\chi}_2^0$ is too small to reproduce the dilepton excess, however its production can be boosted if coloured sparticles subsequently decay into $\tilde{\chi}_2^0$. The explanation of the dilepton excess in terms of coloured sparticles is consistent with the CMS analysis, since events with jet multiplicity are selected and counted.

In this work we perform a detailed study on the possibility of explaining the dilepton excess with several SUSY models taking into account a comprehensive list of LHC constraints from a number of ATLAS and CMS direct SUSY searches. In order to accurately estimate the LHC constraints and simulate many analyses systematically, we use the automated simulation tool **Atom** [4]. We take a bottom-up approach by considering simplified SUSY models with minimal content of particles at low energy to reproduce the excess optimally. As will be discussed in the following sections, light-flavour squarks and sbottoms are potential candidates that satisfy these criteria. Some of these models have already been studied in earlier works [5, 6].⁴ Here, we will confront our simplified models with various direct SUSY search constraints such that their viability is tested in great detail. We will show that the light-flavour squarks and sbottom models we consider in this paper are strongly constrained when providing a large enough contribution to the dilepton excess.

Our paper is organised as follows. In the next section, we describe the selection criteria of the CMS dilepton analysis. In section 3, we consider SUSY models that can possibly reproduce the required features of the dilepton edge. In section 4, we describe the procedure of our simulation and analysis. We discuss our results and their interpretations in Section 5. Conclusions are drawn in Section 6.

⁴See [7] for a non-SUSY interpretation of the observed excess.

2 CMS dilepton analysis

CMS reported an excess of events in the dilepton plus missing energy channel [1, 2] in the 8 TeV, 19.4 fb^{-1} data. The analysis requires an OSSF lepton pair with $p_T > 20 \text{ GeV}$. It also requires ≥ 2 jets with $p_T > 40 \text{ GeV}$ and $\cancel{E}_T > 150 \text{ GeV}$ or ≥ 3 jets with $p_T > 40 \text{ GeV}$ and $\cancel{E}_T > 100 \text{ GeV}$. The excess is observed in the central region where both leptons satisfy $|\eta_{\text{lep}}| < 1.4$. It exhibits an *edge* in the dilepton invariant mass distribution around $m_{\ell\ell} = 78 \text{ GeV}$. The counting experiment in the $m_{\ell\ell} \in [20, 70] \text{ GeV}$ region shows an excess of ~ 130 events over the Standard Model expectation, which corresponds to a standard deviation of 2.6σ .

3 SUSY interpretations of the dilepton edge

In this paper we consider simplified SUSY models that capture the essence needed for explaining the observed dilepton excess. Generalizations of SUSY models given here are straightforward.

It is known that the OSSF dilepton pair in the decay of the second lightest neutralino $\tilde{\chi}_2^0$ via on-shell slepton and off-shell Z exhibit an edge-like shape at

$$m_{\text{edge}} = m_{\tilde{\chi}_2^0} \sqrt{\left(1 - \frac{m_\ell^2}{m_{\tilde{\chi}_2^0}^2}\right) \left(1 - \frac{m_{\tilde{\chi}_1^0}^2}{m_\ell^2}\right)} : \quad \tilde{\chi}_2^0 \rightarrow \tilde{\ell}^\pm \ell^\mp \rightarrow \ell^\pm \ell^\mp \tilde{\chi}_1^0, \quad (1)$$

$$m_{\text{edge}} = m_{\tilde{\chi}_2^0} - m_{\tilde{\chi}_1^0} : \quad \tilde{\chi}_2^0 \rightarrow \ell^\pm \ell^\mp \tilde{\chi}_1^0, \quad (2)$$

respectively, in the $m_{\ell\ell}$ distribution. In order to obtain a large enough production cross section to fit the excess and to have ≥ 2 high p_T jets required in the event selection, we consider production of coloured SUSY particles, which may subsequently decay into $\tilde{\chi}_2^0$. In this paper we consider two scenarios: light-flavour squark and sbottom production.

3.1 Squark scenarios

In the squark scenario, we consider the production of pairs of light-flavour squarks. This scenario assumes the first two generations of squarks (both left and right-handed) to be mass degenerate and within the reach of the LHC, whilst the third generation squarks and gluinos are decoupled. We also assume that the second lightest neutralino is mostly Wino-like or an admixture of Wino and Higgsinos and the lightest neutralino is mostly Bino-like. In this setup the lighter chargino, $\tilde{\chi}_1^\pm$, is naturally introduced as a $SU(2)_L$ partner of the $\tilde{\chi}_2^0$ and their masses have to be close to each other. Since the right-handed squarks do not couple to the Wino and only very weakly couple to the Higgsinos, they decay predominantly into a quark and the $\tilde{\chi}_1^0$, whereas the left-handed squarks can decay to either $\tilde{\chi}_1^\pm$, $\tilde{\chi}_2^0$ or $\tilde{\chi}_1^0$ depending on the Wino-Higgsino mixing in the $\tilde{\chi}_1^\pm$ and $\tilde{\chi}_2^0$.

We consider two models according to the $\tilde{\chi}_1^\pm$ and $\tilde{\chi}_2^0$ decay modes. The first model is the *on-shell slepton* model, where we assume the right-handed selectron and smuon in the low energy spectrum so that the $\tilde{\chi}_2^0$ decays predominantly into an OSSF lepton pair and the $\tilde{\chi}_1^0$ via the on-shell slepton. We decouple the left-handed slepton doublets, $(\tilde{\nu}_L, \tilde{\ell}_L)$, to maximise the signal rate, otherwise the $\tilde{\chi}_2^0$ could also decay into a pair of neutrinos and the $\tilde{\chi}_1^0$ via the on-shell $\tilde{\nu}_L$.⁵

Any models that lead to multi-lepton final states are severely constrained by the multi-lepton plus missing energy searches [10]. To avoid these constraints a large branching ratio of the $\tilde{q}_L \rightarrow q\tilde{\chi}_1^0$ mode is necessary in this model. We assume

$$BR(\tilde{q}_L \rightarrow q + \tilde{\chi}_1^\pm/\tilde{\chi}_2^0/\tilde{\chi}_1^0) = 10/5/85 \%. \quad (3)$$

This can be achieved if $\tilde{\chi}_1^\pm$ and $\tilde{\chi}_2^0$ have large Higgsino components because the squarks couple to the Higgsinos with small Yukawa couplings. We will see in section 5.1 that our conclusion is not sensitive to variations of the branching ratios.

In the squark with on-shell slepton model we then have the following cascade decays

$$\begin{aligned} \tilde{q}_L \rightarrow q\tilde{\chi}_2^0 \rightarrow q\ell^\pm\tilde{\ell}^\mp &\rightarrow q\ell^\pm\ell^\mp\tilde{\chi}_1^0 : & 5 \%, \\ \tilde{q}_L \rightarrow q\tilde{\chi}_1^\pm \rightarrow q\nu\tilde{\ell}^\pm &\rightarrow q\nu\ell^\pm\tilde{\chi}_1^0 : & 10 \%, \\ &\tilde{q}_L \rightarrow q\tilde{\chi}_1^0 : & 85 \%, \\ &\tilde{q}_R \rightarrow q\tilde{\chi}_1^0 : & 100 \%. \end{aligned}$$

If one of the pair produced squarks undergoes the first decay chain, the final state may contain an OSSF dilepton plus two energetic jets, and such events can contribute to the CMS dilepton excess.

The second model we consider in this paper is the *off-shell Z* model, where the $\tilde{\chi}_2^0$ decays via the off-shell Z into an OSSF dilepton pair and the $\tilde{\chi}_1^0$. Unlike in the on-shell slepton model we here need a large branching ratio of $\tilde{q}_L \rightarrow q\tilde{\chi}_2^0$ such that the small leptonic branching ratio of the off-shell Z into electrons and muons (about 6 %) is compensated. We assume

$$BR(\tilde{q}_L \rightarrow q + \tilde{\chi}_1^\pm/\tilde{\chi}_2^0/\tilde{\chi}_1^0) = 66/33/1 \%, \quad (4)$$

which can be realised by assuming $\tilde{\chi}_1^\pm$ and $\tilde{\chi}_2^0$ are Wino-like. In the squark with off-shell Z model we have the following decay chains

$$\begin{aligned} \tilde{q}_L \rightarrow q\tilde{\chi}_2^0 \rightarrow qf\bar{f}\tilde{\chi}_1^0 \text{ (via } Z^*) &: & 33 \%, \\ \tilde{q}_L \rightarrow q\tilde{\chi}_1^\pm \rightarrow qf\bar{f}'\tilde{\chi}_1^0 \text{ (via } W^*) &: & 66 \%, \\ &\tilde{q}_L \rightarrow q\tilde{\chi}_1^0 : & 1 \%, \\ &\tilde{q}_R \rightarrow q\tilde{\chi}_1^0 : & 100 \%. \end{aligned}$$

⁵In our setup the $\tilde{\chi}_2^0$ decays predominantly into muon pairs through the Higgsino component of the $\tilde{\chi}_2^0$.

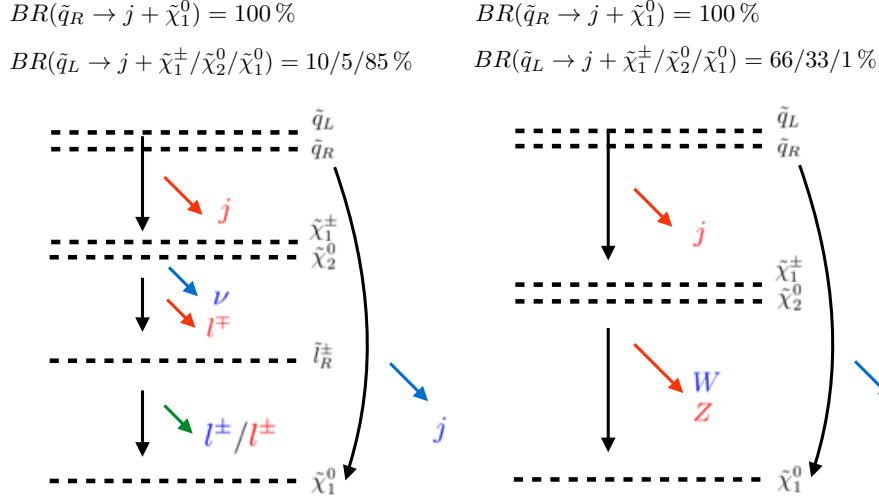


Figure 1: Decay chains of squark scenarios (*left*: on-shell slepton model, *right*: off-shell Z model).

The signal events can be obtained if one of the pair produced squarks undergoes the first decay chain and the $\tilde{\chi}_2^0$ decays via the Z^* into the dilepton pair and the $\tilde{\chi}_1^0$. A schematic picture of the squark scenarios is shown in Fig. 1.

3.2 Sbottom scenarios

Another way of interpreting the CMS dilepton excess is to assume that the observed dileptons in the excessive events come from cascade decays of bottom squarks. Unlike in the squark scenario, the decay mode to charginos, $\tilde{b}_1 \rightarrow t\tilde{\chi}_1^\pm$, is kinematically forbidden if $m_{\tilde{b}_1} < m_t + m_{\tilde{\chi}_1^\pm}$. We consider this case because the decay mode to charginos is more constrained due to emergence of top quarks. Similarly to the squark scenario we consider *on-shell slepton* and *off-shell Z* models according to the $\tilde{\chi}_2^0$ decay mode.

In the on-shell slepton scenario the $\tilde{\chi}_2^0$ may decay either via a right-handed charged slepton or a left-handed charged slepton and sneutrino. We will treat these two cases separately in our analysis.

If the mediating slepton is right-handed, $\tilde{\chi}_2^0$ predominantly decays into two charged leptons and $\tilde{\chi}_1^0$, and the events tend to have more than two leptons in the final state. Such models are severely constrained by the multi-lepton plus missing energy searches as we have previously discussed. To avoid these constraints, we assume 70% of sbottoms decay into a bottom quark and a $\tilde{\chi}_1^0$ and the rest of sbottoms decay into a bottom quark and a $\tilde{\chi}_2^0$. This situation can be achieved if $\tilde{\chi}_2^0$ is Wino-like and \tilde{b}_1 has a large component of \tilde{b}_R . We have the following decay chains in the sbottom with on-shell slepton model.

$$\begin{aligned} \tilde{b}_1 \rightarrow b\tilde{\chi}_2^0 \rightarrow b\ell^\pm\tilde{\ell}^\mp \rightarrow b\ell^\pm\ell^\mp\tilde{\chi}_1^0 &: 30\%, \\ \tilde{b}_1 \rightarrow b\tilde{\chi}_1^0 &: 70\%. \end{aligned}$$

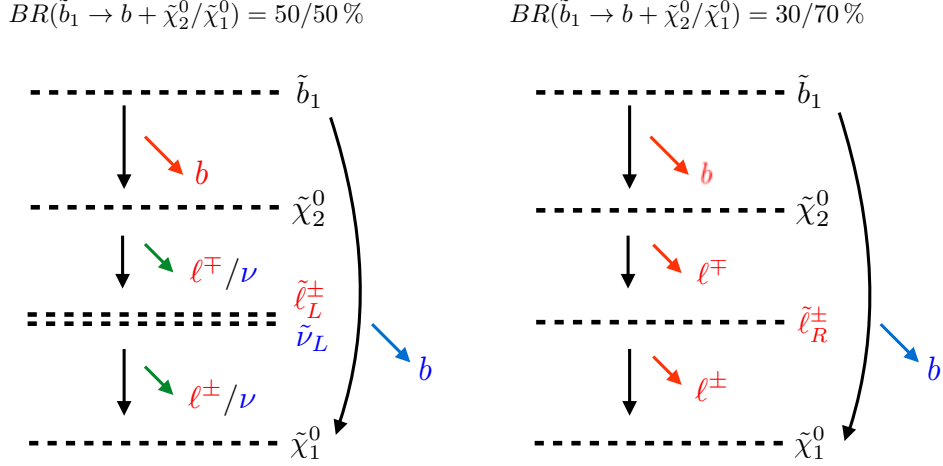


Figure 2: Decay chains of on-shell slepton mediated sbottom scenarios (*left*: left-handed slepton model, *right*: right-handed slepton model).

In the case where the mediating slepton is left-handed, sneutrinos are introduced as $SU(2)$ partners of charged sleptons. We assume sneutrinos and charged sleptons are mass degenerate and $\tilde{\chi}_2^0$ decays democratically into charged sleptons and sneutrinos.

$$\begin{aligned}
 \tilde{b}_1 &\rightarrow b\tilde{\chi}_2^0 \rightarrow b\ell^\pm\tilde{\ell}^\mp \rightarrow b\ell^\pm\ell^\mp\tilde{\chi}_1^0 : & 25\%, \\
 \tilde{b}_1 &\rightarrow b\tilde{\chi}_2^0 \rightarrow b\nu\tilde{\nu} \rightarrow b\nu\nu\tilde{\chi}_1^0 : & 25\%, \\
 \tilde{b}_1 &\rightarrow b\tilde{\chi}_1^0 : & 50\%.
 \end{aligned}$$

The schematic picture of these cases is shown in Fig. 2.

Let us discuss the off-shell Z model for the sbottom scenario. Analogous to the squark with off-shell Z model, we need sbottoms to have a sizeable decay branching ratio to $\tilde{\chi}_2^0$ in order to have large enough dilepton event rates. One way to realise this situation is to have a Higgsino-like $\tilde{\chi}_2^0$, a mostly right-handed \tilde{b}_1 and to assume a large sbottom-bottom-Higgsino coupling due to a large $\tan\beta$. It is shown in [6] that for $\tan\beta = 50$, $m_{\tilde{b}_1} \simeq 330$ GeV and a Higgsino mass parameter $\mu \simeq 290$ around 44% of sbottoms decay to the roughly mass-degenerate $\tilde{\chi}_2^0$ and $\tilde{\chi}_3^0$. This model point predicts about $1\text{-}\sigma$ less events than the central fit without being excluded. In order to explore in more detail the parameter region that could possibly contribute to the excess, we expand the study of this scenario by varying the parameters M_1 , μ and $m_{\tilde{b}_1}$, while fixing $\tan\beta = 50$. The mass spectrum and particle decay branching ratio of this simplified model are calculated using **SPheno** [8, 9].

Alternatively one can obtain a large branching ratio of sbottom decaying to $\tilde{\chi}_2^0$ by assuming \tilde{b}_1 is left-handed and $\tilde{\chi}_2^0$ is Wino-like. Due to $SU(2)$ gauge invariance a left-handed top squark, \tilde{t}_1 , is necessarily included in the low energy spectrum. For simplicity, we assume $m_{\tilde{b}_1} = m_{\tilde{t}_1}$. We consider the following decay chains for the left-handed sbottom

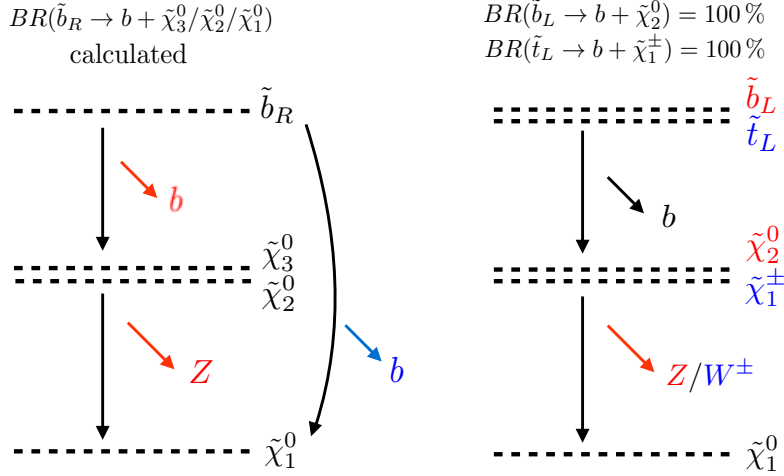


Figure 3: Decay chains of off-shell Z mediated sbottom scenarios (*left*: right-handed sbottom model, *right*: left-handed sbottom model).

with off-shell Z model.

$$\begin{aligned}
 \tilde{b}_1 &\rightarrow q\tilde{\chi}_2^0 \rightarrow qf\bar{f}\tilde{\chi}_1^0 \text{ (via } Z^*) : & 100\%, \\
 \tilde{t}_1 &\rightarrow q\tilde{\chi}_1^\pm \rightarrow qf\bar{f}'\tilde{\chi}_1^0 \text{ (via } W^*) : & 100\%.
 \end{aligned}$$

A schematic picture of the off-shell Z sbottom scenarios is shown in Fig. 3.

The squark and sbottom scenarios are the priorities of this work, but let us also touch on the possibilities of explaining the dilepton excess with the remaining coloured sparticles in SUSY, namely gluino and stop. Gluinos can decay into $\tilde{\chi}_2^0$ via an intermediate squark, not much different from the squark or sbottom scenario other than a larger jet multiplicity. For stop, its decay into a top quark would lead to an extra lepton that plays no role at explaining the dilepton excess. It is not clear how gluino or stop could explain the dilepton excess without inducing additional jet or leptonic constraints, and hence we are not going to study these scenarios further in this work.

4 The simulation setup

In this section we describe our procedure to calculate the contribution to the CMS dilepton excess and the constraints from other ATLAS and CMS SUSY searches.

The production cross section, σ_{prod} , for light-flavour squarks is calculated using **Prospino** 2 [11] with the gluino mass set to 3.5 TeV. For the sbottom cross section we use results from the LHC SUSY Cross Section Working Group based on [12]. We create SLHA files of our simplified models for the event generation and pass them to **Pythia** 6.4 [13] to generate a total number of $10 \cdot \sigma_{\text{prod}} \cdot \mathcal{L}$, with maximal $5 \cdot 10^5$, events, where $\mathcal{L} = 19.4 \text{ fb}^{-1}$ is the integrated luminosity at the CMS dilepton analysis. We then run **Atom** [4] on the

channel	search for	arXiv or CONF-ID	refs
$2-6j + 0\ell + \cancel{E}_T$	\tilde{q}, \tilde{g}	ATLAS-CONF-2013-047 1405.7875	[18] [19]
$2b + 0\ell + \cancel{E}_T$	\tilde{t}, \tilde{b}	1308.2631	[20]
$4j + 1\ell + \cancel{E}_T$	\tilde{t}	ATLAS-CONF-2013-037	[21]
$\geq 2j + \geq 1\ell + \cancel{E}_T$	\tilde{q}, \tilde{g} (1 or 2ℓ)	ATLAS-CONF-2013-062	[22]
$2j + 2\ell + \cancel{E}_T$	dilepton edge	CMS-PAS-SUS-12-019	[1, 2]
$2j + \ell^\pm \ell^\pm + \cancel{E}_T$	$\tilde{q}, \tilde{g}, \tilde{t}, \tilde{b}$ (SS lepton)	ATLAS-CONF-2013-007	[23]
$2j + 2\ell + \cancel{E}_T$	$\tilde{t}(2\ell)$	ATLAS-CONF-2013-048 1403.4853	[24] [25]
$2, 3\ell + \cancel{E}_T$	$\tilde{\chi}^\pm, \tilde{\chi}^0, \tilde{\ell}$	1404.2500 1405.7570	[26] [27]
$3\ell + \cancel{E}_T$	$\tilde{\chi}^\pm, \tilde{\chi}^0$	1402.7029	[28]
$\geq 3\ell + \cancel{E}_T$	$\tilde{\chi}^\pm, \tilde{\chi}^0$	CMS-PAS-SUS-13-002	[10]

Table 1: LHC searches used in this paper to test the viability of the simplified models.

generated HepMC event files to estimate the efficiencies, ϵ , of the signal regions defined in all the ATLAS and CMS analyses that will be used in this work. The application examples and validation of **Atom** is found in [14, 15, 16]. We have implemented the CMS dilepton analysis in **Atom** and validated it using the cut-flow tables given by the CMS collaboration based on the $\tilde{b}_1 \rightarrow b\tilde{\chi}_2^0 \rightarrow b\ell^+\ell^-\tilde{\chi}_1^0$ simplified model. The comparison in the number of expected signal events calculated by **Atom** and CMS is shown in Appendix A. We also cross-checked some of the analyses with another simulation tool **CheckMATE** [17].

From the obtained cross section and efficiency, the SUSY contribution to the CMS dilepton excess is calculated as $N_{\ell\ell} = \sigma_{\text{eff}} \cdot \mathcal{L}$, where the effective cross section, σ_{eff} , is defined as the cross section after the event selection: $\sigma_{\text{eff}} = \epsilon \cdot \sigma_{\text{prod}}$. For the other ATLAS and CMS analyses the 95% CL upper limit on σ_{eff} , σ_{UL} , is reported for each signal region by the collaborations. We define a useful measure for exclusion by $R = \sigma_{\text{eff}}/\sigma_{\text{UL}}$. If $R > 1$ is found for one of the signal regions, the model is likely to be excluded, although one needs to combine all the signal regions statistically to draw a definite conclusion. However, we do not attempt to combine these signal regions because there are non-trivial correlations among them which originate from the uncertainties on *e.g.* the jet energy scale, the lepton efficiency and luminosity, and it is not possible for us to combine the signal regions correctly. Instead, in the next section we will look at the exclusion measure R individually to understand which signal regions are sensitive to the model points.

In Table 1 we list the ATLAS and CMS analyses we consider in this work. We include the multi-jet [18, 19] and di- b jet [20] analyses, jets plus single [21] or two lepton [1, 2, 23] (including same-sign (SS) dilepton [23]) analyses [22] and multi-lepton analyses [26, 27, 10, 28]. In the next section we investigate whether the SUSY models can fit the CMS dilepton excess taking the constraints from these analyses into account.

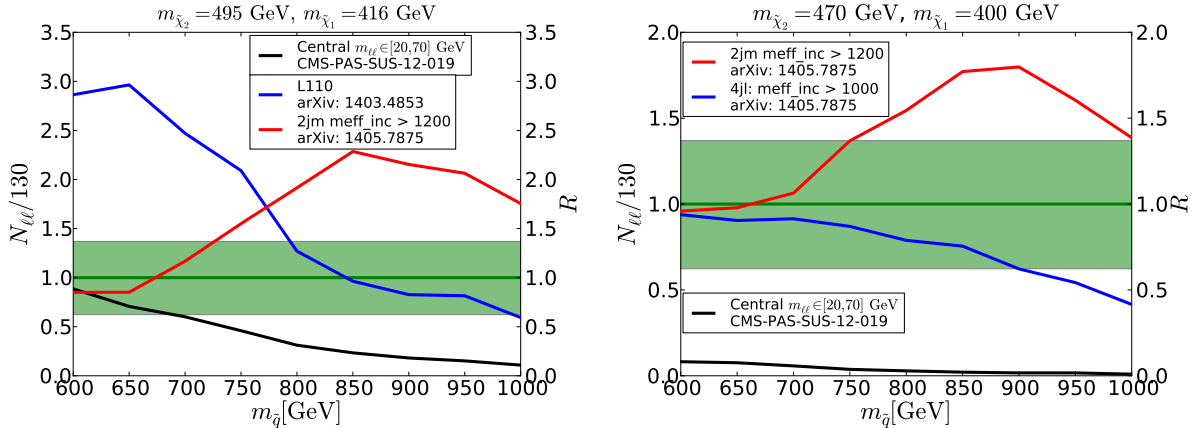


Figure 4: Signal rate and R -values for the squark models. The left panel presents the intermediate slepton, the right panel the off-shell Z scenario.

5 Results

5.1 Squark scenarios

In Fig. 4 we show the results of our numerical calculation for the squark scenario. In the plots the black curves represent the SUSY contribution, $N_{\ell\ell}$, normalised by the best fit value 130. The green bands correspond to the 1σ region of the fit. In the same plots we show also the exclusion measure, R , for a few signal regions that are particularly sensitive to the models. The region where any R is greater than 1 is strongly disfavoured.

In the left panel of Fig. 4 we show $N_{\ell\ell}/130$ and R as functions of $m_{\tilde{q}}$ for the squark with on-shell slepton model. We fix $m_{\tilde{\chi}_2^0} = 495 \text{ GeV}$ and $m_{\tilde{\chi}_1^0} = 416 \text{ GeV}$. For these masses, there are no constraints from the chargino-neutralino direct searches. The right-handed slepton mass is fixed at 450 GeV such that m_{edge} in Eq. (1) is 78 GeV, which is the optimal value for the CMS dilepton excess.

As can be seen, this model can fit the excess only in the region where $m_{\tilde{q}} \lesssim 650 \text{ GeV}$. However, this region is strongly disfavoured by the L110 signal region (shown in the blue curve) in the ATLAS stop search [25]. This signal region requires the same final state ($2j + 2\ell + \cancel{E}_T$) as the CMS dilepton analysis, in particular an OS lepton pair with $p_T > 25 \text{ GeV}$ and at least two jets with $p_T > 20 \text{ GeV}$. The condition $m_{T2} > 110 \text{ GeV}$ is also imposed, which is very effective to reduce the $t\bar{t}$ and $WW + \text{jets}$ backgrounds. One can see that the sensitivity of this signal region decreases as the $m_{\tilde{q}}$ increases due to the reduction of the production cross section. Nevertheless, the signal rate in the dilepton excess also decreases in the same way since these analyses employ similar event selection. Consequently there is no region in the plot where the SUSY events can fit the dilepton excess avoiding the exclusion from the other searches. This conclusion is robust against our assumption on the branching ratios, $Br(\tilde{q}_L \rightarrow q + \tilde{\chi}_1^\pm/\tilde{\chi}_2^0/\tilde{\chi}_1^0) = 10/5/85\%$, since the

L110 signal region constrains the same channel as in the CMS dilepton analysis.

One can also see that in the $m_{\tilde{q}} > 680$ GeV region, the 2jm signal region in the ATLAS multi-jet search [19] becomes sensitive and rules out the model points. This signal region is characterised by the requirement of at least two jets with $p_T > 130$ and 60 GeV and a moderately large effective mass, $m_{\text{eff}} \equiv \sum_i |p_{T_i}^{j40}| + \cancel{E}_T > 1200$ GeV, where $p_{T_i}^{j40}$ is the i -th high p_T jet with $p_T > 40$ GeV. The events with an electron or muon with > 10 GeV are rejected in this analysis. The 2jm signal region targets the $\tilde{q}\tilde{q} \rightarrow q\tilde{\chi}_1^0 q\tilde{\chi}_1^0$ topology, which is indeed the dominant event topology in this model since $Br(\tilde{q}_R \rightarrow q\tilde{\chi}_1^0) = 100\%$ and $Br(\tilde{q}_L \rightarrow q\tilde{\chi}_1^0) = 85\%$.⁶ Due to the harsh cut on the m_{eff} , the 2jm signal region is sensitive to the models with large mass gaps between \tilde{q} and $\tilde{\chi}_1^0$. This is the reason why the sensitivity increases as $m_{\tilde{q}}$ increases until the point ($m_{\tilde{q}} \simeq 850$ GeV) at which a rapid degradation of the squark production cross section finally turns the sensitivity down.

In the right panel of Fig. 4, we plot the $N_{\ell\ell}/130$ and R as functions of $m_{\tilde{q}}$ for the squark with off-shell Z model, where we fix $m_{\tilde{\chi}_2^0} = 478$ GeV and $m_{\tilde{\chi}_1^0} = 400$ GeV so that m_{edge} in Eq. (2) is 78 GeV. One can see that the SUSY contribution is too small to account for the dilepton excess, whilst this region is severely constrained by the 2jm and 4jl signal regions in the ATLAS multi-jet search [19]. Compared to the on-shell slepton model, the rate of an OSSF lepton from a squark cascade decay is small: $Br(\tilde{q}_L \rightarrow q\tilde{\chi}_2^0) \cdot Br(\tilde{\chi}_2^0 \rightarrow Z^*\tilde{\chi}_1^0) \cdot Br(Z^* \rightarrow \ell^+\ell^-) \simeq 0.33 \cdot 1 \cdot 0.06 \simeq 2\%$, though we took a maximal value 33% for $Br(\tilde{q}_L \rightarrow q\tilde{\chi}_2^0)$ assuming $\tilde{\chi}_2^0$ and $\tilde{\chi}_1^\pm$ to be Wino-like. Instead, $\tilde{\chi}_2^0$ and $\tilde{\chi}_1^\pm$ have large branching ratio to hadronic modes via Z^* and W^* which makes the off-shell Z model more prone to be excluded by the ATLAS multi-jet search [19] compared to the on-shell slepton model due to the lepton veto cut in the analysis. The 2jm signal region constrains mostly $\tilde{q}_R\tilde{q}_R \rightarrow q\tilde{\chi}_1^0 q\tilde{\chi}_1^0$ topology and the sensitivity peaks around $m_{\tilde{q}} \simeq 900$ GeV with $m_{\tilde{\chi}_1^0} = 400$ GeV, similarly to the on-shell slepton model. On the other hand, the 4jm signal region requires at least 4 jets ($p_T > 130, 60, 60, 60$ GeV) and looks at the jets not only from the squark decay, $\tilde{q} \rightarrow j\tilde{\chi}$ ($\tilde{\chi} = \tilde{\chi}_1^0, \tilde{\chi}_2^0$ or $\tilde{\chi}_1^\pm$), but also from hadronic $\tilde{\chi}_1^\pm$ and $\tilde{\chi}_2^0$ decays and initial state radiation. Due to the milder cut $m_{\text{eff}} > 1000$ GeV, the sensitivity peaks at a much lower squark mass.

We conclude that for the squark models it is very difficult to fit the observed CMS dilepton excess if the ATLAS stop search [25] and the ATLAS multi-jet search [19] are both considered.

5.2 Sbottom scenarios

In this section we present the results for the sbottom scenarios, starting with the on-shell left-handed slepton model. In Fig. 5 we show $N_{\ell\ell}/130$ and R of the most constraining

⁶ We note that in [19] ATLAS does not exclude the region where $m_{\tilde{\chi}_1^0} = 416$ GeV in the squark-neutralino simplified model. We, on the other hand, exclude this neutralino mass for a certain range of the squark mass (see Fig. 4 (left)). This is because our squark production cross section is larger than the ATLAS's value since we set the gluino mass at 3.5 TeV in which the contribution from the gluino exchange diagram is still sizeable.

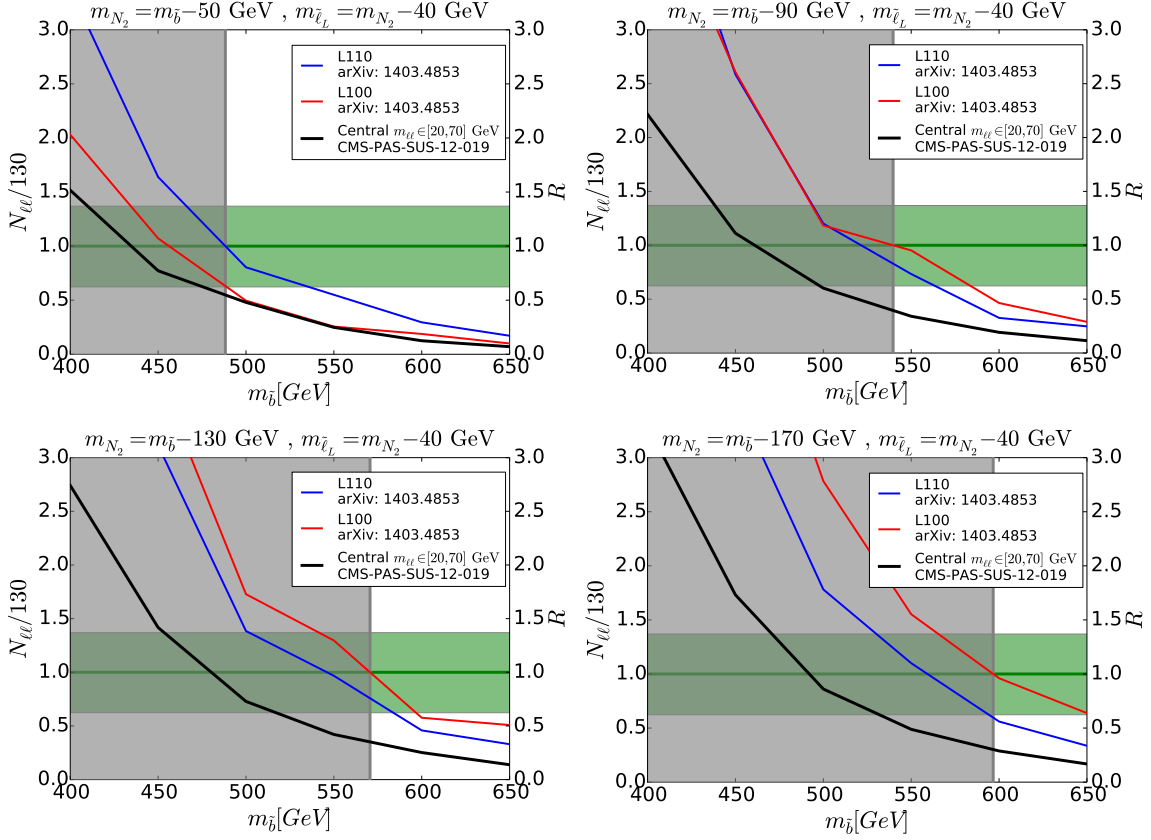


Figure 5: Signal rate and R -values for the on-shell left-handed slepton mediated sbottom models.

signal regions as functions of $m_{\tilde{b}_1}$. As discussed previously, we assume $m_{\tilde{\chi}_2^0} < m_{\tilde{b}_1} - m_t$ to avoid tops in the decay chains that would lead to more stringent constraints. Within this condition we examine four different mass gaps: $\Delta m \equiv m_{\tilde{b}_1} - m_{\tilde{\chi}_2^0} = 50, 90, 130$ and 170 GeV. The left-handed slepton mass is fixed at $m_{\tilde{\ell}_L} = m_{\tilde{\chi}_2^0} - 40$ GeV and $m_{\tilde{\chi}_1^0}$ is set for each combination of $m_{\tilde{\chi}_2^0}$ and $m_{\tilde{\ell}_L}$ such that m_{edge} in Eq. (1) is 78 GeV. The intermediate slepton can either be a sneutrino or a charged slepton and the branching ratio of $\tilde{\chi}_2^0$ into these two states is assumed to be equal. Therefore, only half of the produced $\tilde{\chi}_2^0$ decay into an OSSF dilepton and a $\tilde{\chi}_1^0$.

In Fig. 5 we see that a good fit can be obtained for sbottom masses between 420 and 520 GeV, depending on Δm . However, these model points are strongly disfavoured by the L100 and L110 signal regions of the ATLAS stop search [25]. The event selection in the L100 signal region is very similar to the L110 signal region which we briefly described in the previous subsection. The difference is that in the L100 signal region the lepton p_T requirement is raised to $(p_T^{\ell_1}, p_T^{\ell_2}) > (100, 50)$ GeV and $m_{T2} > 100$ GeV is imposed. As the lepton p_T requirement is raised with respect to L110, L100 is especially sensitive to larger mass gaps.

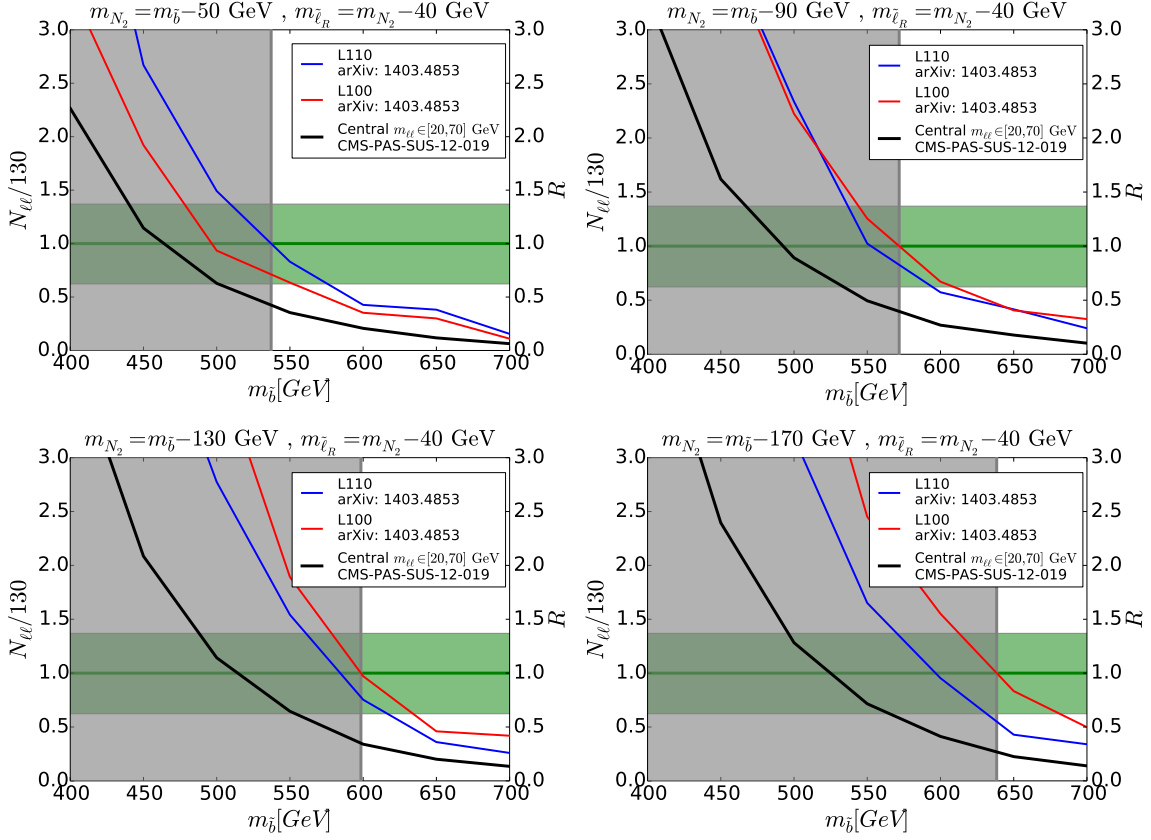


Figure 6: Signal rate and R -values for the on-shell right-handed slepton mediated sbottom models.

In Fig. 6 we show the contribution to the excess and the constraints from other searches in the on-shell right-handed slepton model for the four different Δm , similarly to Fig. 5. In this scenario $\tilde{\chi}_2^0$ decays into an OSSF dilepton and a $\tilde{\chi}_1^0$ with the branching ratio of 100%. As can be seen, the results are similar to the left-handed slepton case and the region where the model gives a good fit is strongly disfavoured by the L110 and L100 signal regions of the ATLAS stop search. The similarity of the results amongst the left- and right-handed slepton scenarios can be understood because L110 and L100 constrain the same final state ($2j + 2\ell + \cancel{E}_T$) as that is targeted in the CMS dilepton analysis and the kinematics of the dilepton events are similar between these scenarios. We conclude that it is difficult to attribute the CMS dilepton excess to the sbottom with on-shell slepton models if the constraint from the ATLAS stop search [25] is taken into account.

We now turn to the sbottom with off-shell Z models. The first model we investigate is the right-handed sbottom model where $\tilde{\chi}_2^0$ and $\tilde{\chi}_3^0$ are mostly Higgsino-like and $\tilde{\chi}_1^0$ is mostly Bino-like. In this model the masses of three lightest neutralinos are calculated from the parameters, μ , M_1 and $\tan\beta$, fixing M_2 at 3.5 TeV. Since we assume $\mu > M_1$, we have $m_{\tilde{\chi}_3^0} \sim m_{\tilde{\chi}_2^0} \sim \mu$ and $m_{\tilde{\chi}_1^0} \sim M_1$ and both $\tilde{\chi}_2^0$ and $\tilde{\chi}_3^0$ can contribute to the excess through

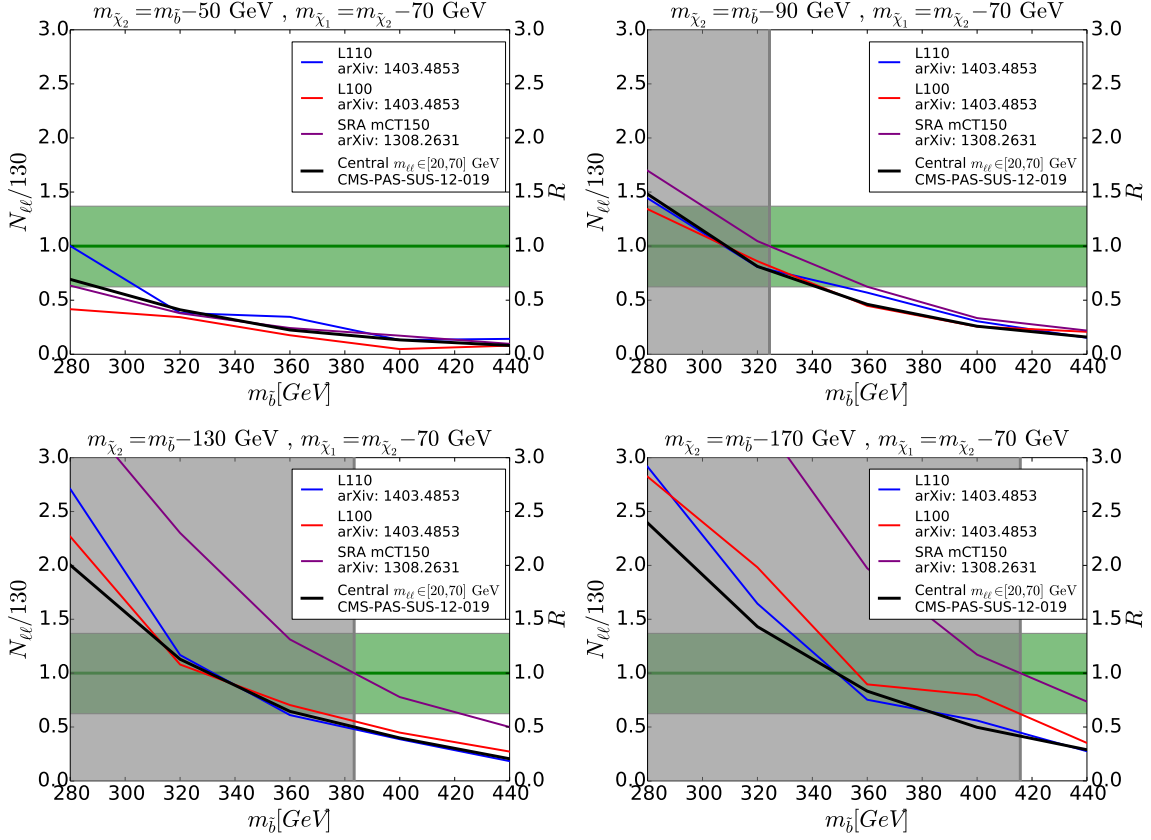


Figure 7: Signal rate and R -values for the off-shell Z -mediated right-handed sbottom-higgsino models.

their decays into an off-shell Z boson and a $\tilde{\chi}_1^0$. The decay rate of the sbottom into the Higgsino states is dictated by the sbottom-bottom-Higgsino coupling which is proportional to $\tan\beta$. In order to have a large signal rate, we take $\tan\beta = 50$ in our numerical scan. We again examine four different mass gaps $\Delta m = 50, 90, 130,$ and 170 GeV between the sbottom and $\tilde{\chi}_2^0$. To this end we vary μ such that $\tilde{\chi}_2^0$ takes the desired mass set by Δm . M_1 is chosen such that $m_{\tilde{\chi}_2^0} - m_{\tilde{\chi}_1^0} = 70$ GeV. The mass of the lightest sbottom is calculated from given parameters fixing the left-handed third generation squarks mass, $m_{\tilde{Q}_3}$, at 1.5 TeV. A table with parameter values for each model point can be found in the Appendix B.

In Fig. 7 we show our results again in terms of $N_{\ell\ell}/130$ and R . First we note that the strong constraint from L100 and L110 observed in the on-shell slepton models is relaxed. To understand this we compare the distributions of m_{T2} , a kinematical variable used both in the L100 and L110 signal regions, between the on-shell right-handed slepton (blue) and off-shell Z models (red) in Fig. 8 at similar mass spectra. We take $(m_{\tilde{b}_1}, m_{\tilde{\chi}_2^0}) = (400, 230)$ GeV and fix $m_{\tilde{\chi}_1^0}$ such that $m_{\text{edge}} \simeq 78$ GeV for both models. For the on-shell slepton model we take $m_{\tilde{\ell}} = 190$ GeV. In Fig. 8 we see that the off-shell Z model tends to give

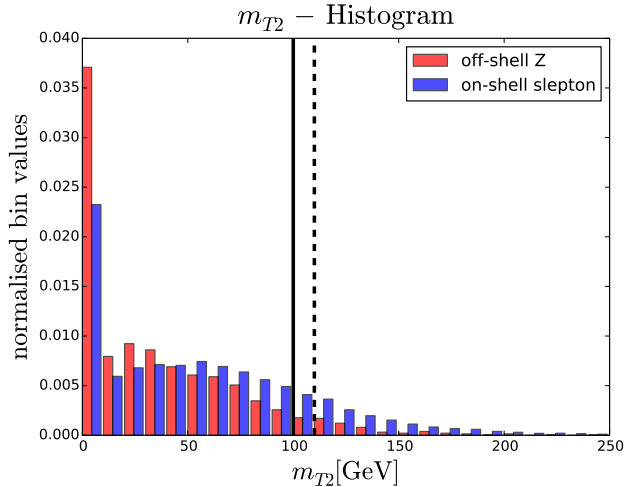


Figure 8: Histogram of m_{T2} -distribution for sbottom production for both the off-shell Z and on-shell RH-slepton mediated case. The sbottom mass is 400 GeV and $m_{\tilde{\chi}_2^0} = 230$ GeV. For the off-shell slepton mediated case we have $m_{\tilde{\mu}_R} = 190$ GeV and $m_{\tilde{\chi}_1^0} = 151$ GeV. The black vertical line indicates the cut for the limiting signal region SRA mCT150.

smaller m_{T2} compared to the on-shell slepton model. The solid (dashed) vertical black line represents the event selection cut on the m_{T2} variable employed in the L100 (L110) signal region. As can be seen, the off-shell Z model is less sensitive to the the L100 and L110 signal regions than the on-shell slepton model.

What can also be seen from Fig. 7 is that for $\Delta m > 90$ GeV the SRA mCT150 signal region in the ATLAS di-bottom analysis [20] is constraining and most of the preferred region of the dilepton excess is indeed disfavoured by this signal region. This signal region looks for two energetic b -jets with $p_T > 130$ and 50 GeV in events with $m_{CT} > 150$ GeV⁷ and $\cancel{E}_T > 150$. Events containing an electron ($p_T > 7$ GeV) or a muon ($p_T > 6$ GeV) are rejected in this analysis. This signal region is more constraining for larger Δm because the event selection requires two energetic b -jets.

For $\Delta m = 50$ and 90 GeV we find the regions where the observed excess can be explained at 1- σ level without $R > 1$ from other searches. This result is consistent with the findings reported in [6]. However these regions are already in tension with other searches. In particular the ATLAS stop search [25] and the ATLAS di-bottom search [20] give $R \lesssim 1$ in these regions.

In Fig. 9 we show $N_{\ell\ell}/130$ and R as functions of $m_{\tilde{b}_1}$ in the left-handed sbottom model where $\tilde{\chi}_2^0$ ($\tilde{\chi}_1^\pm$) is assumed to be Wino-like and decays predominantly to an off-shell Z (W) and a Bino-like $\tilde{\chi}_1^0$. We again show the results for four different mass gaps and

⁷ $m_{CT} \equiv \sqrt{(E_T^{b_1} + E_T^{b_2})^2 - (\mathbf{p}_T^{b_1} - \mathbf{p}_T^{b_2})^2}$, where E_T and \mathbf{p}_T are the transverse energy and the transverse momentum vector, respectively.

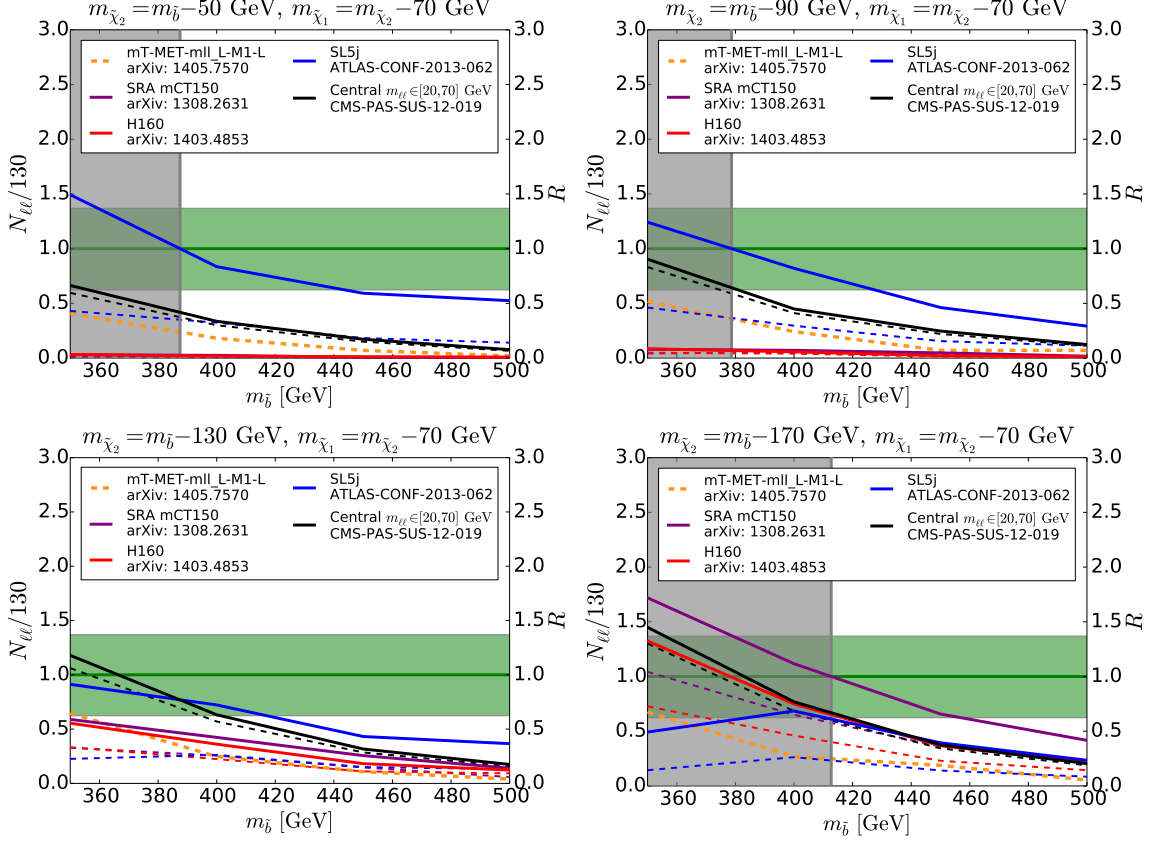


Figure 9: Signal rate and R -values for the off-shell Z -mediated left-handed sbottom model. Pure sbottom production is indicated by dashed lines and combined sbottom and stop production by solid lines.

fix $m_{\tilde{\chi}_1^0} = m_{\tilde{\chi}_2^0} - 70$ GeV to fit the central value of the counting experiment. As we have mentioned in section 3, we assume the presence of the top squark, \tilde{t}_1 , with $m_{\tilde{t}_1} = m_{\tilde{b}_1}$. The solid curves in Fig. 9 represent the results with both $\tilde{b}_1\tilde{b}_1^*$ and $\tilde{t}_1\tilde{t}_1^*$ production processes. To see the impact of the tilde $\tilde{t}_1\tilde{t}_1^*$ production on the result, we also plot the contribution to $N_{\ell\ell}/130$ and R from $\tilde{b}_1\tilde{b}_1^*$ by dashed curves.

One can see from Fig. 9 that for $\Delta m = 50$ and 90 GeV the model is strongly constrained by the SL5j signal region in the ATLAS jets plus 1-2 lepton analysis [22]. This signal region requires a soft single electron (muon) with $p_T \in [10, 25]$ ($[6, 25]$) GeV and veto additional electron (muon) with $p_T > 10$ (6) GeV. It also requires ≥ 5 jets with $p_T > (180, 25, 25, 25, 25)$ GeV. The SL5j signal region is more sensitive to the $\tilde{t}_1\tilde{t}_1^*$ topology where one of the stops decays hadronically $\tilde{t}_1 \rightarrow b\tilde{\chi}_1^\pm \rightarrow bW^*\tilde{\chi}_1^0 \rightarrow bqq'\tilde{\chi}_1^0$ and the other decays leptonically $\tilde{t}_1 \rightarrow b\tilde{\chi}_1^\pm \rightarrow bW^*\tilde{\chi}_1^0 \rightarrow b\ell\nu\tilde{\chi}_1^0$, because event selection requires a single lepton. We also note that the SL5j signal region becomes less sensitive for larger Δm because the leptons from the stop cascade decay chain are boosted in this case and do

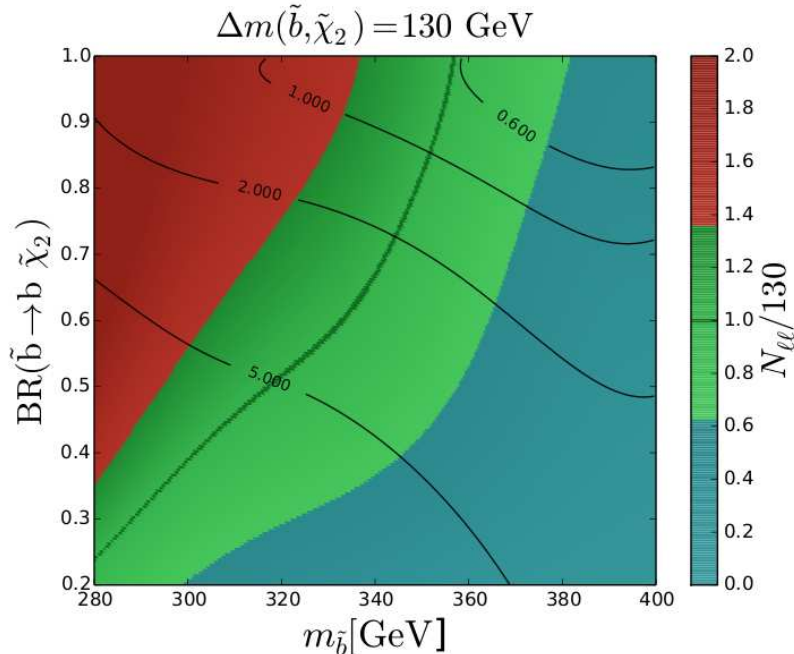


Figure 10: Variation of \tilde{b}_1 branching ratio into $\tilde{\chi}_2^0$ for off-shell Z mediated left-handed sbottom scenario with no stop production. The color indicates $N_{\ell\ell}/130$ and the black curves are lines of constant R_{\max} . Only large wino branching ratios can provide a good fit to the excess.

not pass the low p_T requirement (< 25 GeV) efficiently. However, for larger Δm the SRA mCT150 signal region becomes constraining. In particular the preferred region of the dilepton excess is disfavoured by this signal region at $\Delta m = 170$ GeV.

As a result we find a good fit to the dilepton excess at $\Delta m = 130$ GeV and $m_{\tilde{b}_1} \in [350, 400]$ GeV, although this region is already in tension with the SL5j signal region in the ATLAS jets plus 1-2 lepton analysis. In addition, let us note that there is an additional constrain on the $\tilde{\chi}_1^0 - \tilde{t}_1$ mass plane from CMS single-lepton analysis [29], which is not included in our analysis. This analysis does not use the cut-and-count method but rather uses a BDT multivariate method, which prevents us from implementing this analysis. While recasting this analysis is out of the scope of this work, it is worthwhile to deduce its constraint on our models. Specifically, the exclusion contour on the $\tilde{\chi}_1^0 - \tilde{t}_1$ mass plane with chargino mass fixed at $m_{\tilde{\chi}_1^\pm} = 0.25 m_{\tilde{t}_1} + 0.75 m_{\tilde{\chi}_1^0}$ in the CMS analysis is most relevant to the allowed parameter space in our study ($m_{\tilde{\chi}_1^\pm} \simeq 0.3 m_{\tilde{t}_1} + 0.7 m_{\tilde{\chi}_1^0}$). At $m_{\tilde{t}_1} \simeq 380$ GeV the CMS analysis excludes $m_{\tilde{\chi}_1^0} \lesssim 200$ GeV, whilst $m_{\tilde{\chi}_1^0} = 180$ GeV at $m_{\tilde{t}_1} = 380$ GeV in the bottom left plot ($\Delta m = 130$ GeV) in Fig 9.

It is interesting to note that the difference between the black solid and black dashed curves are small, whereas the difference is large amongst the blue solid and blue dashed curves in the bottom left plot ($\Delta m = 130$ GeV) in Fig 9. This means that the $\tilde{b}_1 \tilde{b}_1^*$ pro-

duction gives the main contribution to the dilepton excess, while the model is disfavoured mainly by the additional $\tilde{t}_1\tilde{t}_1^*$ production. Before concluding our study we show in Fig. 10 the contribution to the dilepton excess and the constraint from other searches in the $m_{\tilde{b}_1}$ versus $BR(\tilde{b}_1 \rightarrow b\tilde{\chi}_2^0)$ plane concerning only the $\tilde{b}_1\tilde{b}_1^*$ production. In this study we assume $BR(\tilde{b}_1 \rightarrow b\tilde{\chi}_1^0) = 1 - BR(\tilde{b}_1 \rightarrow b\tilde{\chi}_2^0)$. The region is divided into 3 colours, red, green and blue, which correspond to under, good and over fit of the dilepton excess, respectively. The R value of the most constraining signal region is shown in the black contours. One can see that a good fit is found for $m_{\tilde{b}_1} \in [340, 380]$ GeV and $BR(\tilde{b} \rightarrow b\tilde{\chi}_2^0) \gtrsim 0.8$ without having $R > 1$ from other searches. Within our exploration we did not find the models where the sbottom is mostly right-handed and $BR(\tilde{b} \rightarrow b\tilde{\chi}_2^0) \gtrsim 0.8$. However, this result indicates that models that have a large cross section of the topology equivalent to $\tilde{b}_1 \rightarrow b\tilde{\chi}_2^0 \rightarrow bZ^*\tilde{\chi}_1^0$ can in principle explain the CMS dilepton excess avoiding constraints from other ATLAS and CMS direct SUSY searches.

6 Conclusions

One straightforward supersymmetric interpretation of the observed dilepton excess by CMS [1, 2] is the cascade decays of light-flavour and bottom squarks. In this paper, we studied and tested the viability of promising SUSY models by deriving constraints on these from various direct SUSY searches using the automated simulation tool **Atom**.

In order to obtain a contribution to the dilepton excess from SUSY events, we considered the decay of the second lightest neutralino, $\tilde{\chi}_2^0$, via either an off-shell Z or an intermediate on-shell slepton. The $\tilde{\chi}_2^0$ itself arises from a light-flavour squark or sbottom decay. We investigated in total six possible simplified models, see figures 1, 2 and 3.

We found that all of these models are already in strong tension with the experimental data once we demand a good fit to the dilepton excess. In particular strong limits arise from an earlier neglected ATLAS stop search [25] with identical final state topology. This analysis alone rules out the interpretation of the excess in terms of an intermediate (left- or right-handed) on-shell slepton for both light squark and sbottom production, see left panel of Fig. 4, Fig. 5 and Fig. 6 respectively. We showed that if multijet plus missing energy searches are taken into account, the off-shell Z scenario with squark production is strongly disfavoured and noted that it is not able to give a sizeable contribution to the dilepton signal region, as can be seen in the right panel of Fig. 4.

We confirmed the result reported in [6] and showed that the right-handed sbottom model with Higgsino-like $\tilde{\chi}_2^0$ and $\tilde{\chi}_3^0$ decaying predominantly into an off-shell Z can explain the dilepton excess at 1- σ level, although the model is already in tension with the ATLAS di-bottom search and the ATLAS stop search, as can be seen in Fig. 7. This tension can be ameliorated if the left-handed sbottom model with Wino-like $\tilde{\chi}_2^0$ is considered. However, the left-handed stop is necessarily introduced in this model and that creates another tension with the ATLAS jets plus 1-2 lepton analysis as be seen in Fig. 9.

We also showed in Fig. 10 that in a simplified model that only has sbottom production

the dilepton excess can be explained avoiding constraints from other searches in the region where $m_{\tilde{b}_1} - m_{\tilde{\chi}_2^0} \sim 130$ GeV, $m_{\tilde{b}} \sim 360$ GeV and $BR(\tilde{b}_1 \rightarrow b\tilde{\chi}_2^0) \gtrsim 0.8$, although we did not find a corresponding model point in the context of the MSSM within our exploration. This results may indicate that a more non-trivial SUSY scenario should be considered to explain the CMS dilepton excess.

Note added: Shortly after this paper was submitted to arXiv, CMS updated their result [2] and reported most of the excessive events are observed associated with at least one b -jet. This new information further disfavours the squark scenario, which does not change our conclusion. Shortly after the CMS update, ATLAS released their new analysis of the jets plus SFOS dilepton channel [30]. They explicitly looked at the signal region employed in the CMS dilepton analysis and did not find any significant excess. This casts a doubt that observed dilepton excess is merely due to the statistical fluctuation or background mismodeling. The next run of the LHC will provide a definitive answer to this question.

A Validation

Here we show the validation results of our implementation of CMS-PAS-SUS-12-019/1502.06031 [1, 2] and the ATLAS stop search with two lepton final state [25].

The benchmark point considered in the CMS analysis has a sbottom of mass 400 GeV decaying via $\tilde{b} \rightarrow \tilde{\chi}_2^0 b$ with 100%. The second lightest neutralino then undergoes an off-shell Z decay with SM branching ratios. We show the good agreement between the CMS results and our implemented analysis in `Atom` in table 2. There, we give the event numbers in the central and forward signal regions as quoted by the CMS collaboration and their ratio to our results obtained with `Atom`.

Additionally, we provide validation results for the stop search because of the strong constraints that we derive from this analysis. The ATLAS benchmark scenario consists of a stop decaying to $\tilde{\chi}_1^\pm + b$ with 100% probability followed by a decay of $\tilde{\chi}_1^\pm$ via a W into $\tilde{\chi}_1^0$ and Standard Model particles. We show our validation in table 3. In this table we present event numbers for the same-flavour (SF) and different-flavour (DF) case as given by ATLAS and their ratio to our results in the column `Atom/Exp`.

$(m_{\tilde{b}}, m_{\tilde{\chi}_2^0}) = (400, 150)$ GeV	Central	<code>Atom/Exp</code>	Forward	<code>Atom/Exp</code>
$N_{\text{jets}} \geq 2$ (no \cancel{E}_T requirement)	242.7 ± 2.8	1.04	34.2 ± 1.1	0.77
$N_{\text{jets}} \geq 3$ (no \cancel{E}_T requirement)	186.2 ± 2.5	1.09	25.6 ± 0.9	0.76
$\cancel{E}_T > 100$ GeV(no N_{jets} requirement)	152.5 ± 2.1	1.03	19.8 ± 0.8	0.98
$\cancel{E}_T > 150$ GeV(no N_{jets} requirement)	85.0 ± 1.5	0.93	10.4 ± 0.5	0.87
Signal region	132.4 ± 2.0	1.031	17.0 ± 0.7	0.937

Table 2: Validation table for our implementation of the CMS-PAS-SUS-12-019/1502.06031 analysis [1, 2] in `Atom`.

$(m_{\tilde{t}}, m_{\tilde{\chi}_1^\pm}, m_{\tilde{\chi}_1^0}) = (400, 390, 195)$ GeV	SF	Atom/Exp	DF	Atom/Exp
$\Delta\phi > 1$	1834.9	1.09	2390.1	1.06
$\Delta\phi_b$	1402.8	1.07	1800.5	1.07
$m_{T2} > 90$ GeV	396.5	1.02	500.0	1.09
$m_{T2} > 120$ GeV	211.8	1.01	284.4	1.1
$m_{T2} > 100$ GeV, $p_{T,\text{jet}} > 100$ GeV	21.7	1.4	35.0	0.99
$m_{T2} > 110$ GeV, $p_{T,\text{jet}} > 20$ GeV	86.0	0.95	116.1	0.89

Table 3: Validation table for our implementation of the ATLAS stop search with two leptons [25] in Atom.

B Parameter Values for pMSSM scan

In table 4 we give additional pMSSM input parameters as well as the sum of the branching ratio of \tilde{b}_1 to $\tilde{\chi}_2^0, \tilde{\chi}_3^0$. These points were used to scan the right-handed sbottom-Higgsino model. Calculation of the physical SUSY masses and branching ratios was done using SPheno [8, 9].

	$\Delta m(\tilde{b}, \tilde{\chi}_2^0) = 50$	$\Delta m(\tilde{b}, \tilde{\chi}_2^0) = 90$	$\Delta m(\tilde{b}, \tilde{\chi}_2^0) = 130$	$\Delta m(\tilde{b}, \tilde{\chi}_2^0) = 170$
$m_{\tilde{b}} = 280$	(229,157,0.48)	(183,157,0.63)	(140,157,0.69)	(96,157,0.63)
$m_{\tilde{b}} = 320$	(270,215,0.48)	(228,215,0.63)	(183,215,0.69)	(140,215,0.67)
$m_{\tilde{b}} = 360$	(307,263,0.46)	(269,263,0.63)	(228,263,0.69)	(183,263,0.7)
$m_{\tilde{b}} = 400$	(345,310,0.46)	(307,310,0.63)	(269,310,0.7)	(228,310,0.71)

Table 4: Additional information about the right-handed sbottom-higgsino model. We give values for $(\mu, m_{\tilde{b}_R}, \sum_{i=2,3} BR(\tilde{b} \rightarrow b N_i))$ for each model point. All masses and mass differences are given in GeV. See text for more details.

Acknowledgment

We are grateful to J. S. Kim, K. Rolbiecki, and J. Tattersall for collaborations during the early stages of this work. P.G. is supported by an ERC grant. S.P.L. is supported by JSPS Research Fellowships for Young Scientists and the Program for Leading Graduate Schools, MEXT, Japan. The work of K.S. was supported in part by the London Centre for Terauniverse Studies (LCTS), using funding from the European Research Council via the Advanced Investigator Grant 267352.

References

- [1] CMS Collaboration [CMS Collaboration], CMS-PAS-SUS-12-019.
- [2] V. Khachatryan *et al.* [CMS Collaboration], arXiv:1502.06031 [hep-ex].
- [3] B. C. Allanach, C. G. Lester, M. A. Parker and B. R. Webber, JHEP **0009** (2000) 004 [hep-ph/0007009].
- [4] I.W. Kim, M. Papucci, K. Sakurai and A. Weiler, “ATOM: Automated Testing Of Models”, in preparation.
- [5] B. Allanach, A. R. Raklev and A. Kvellestad, arXiv:1409.3532 [hep-ph].
- [6] P. Huang and C. E. M. Wagner, Phys. Rev. D **91** (2015) 1, 015014 [arXiv:1410.4998 [hep-ph]].
- [7] B. Allanach, A. Alves, F. S. Queiroz, K. Sinha and A. Strumia, arXiv:1501.03494 [hep-ph].
- [8] W. Porod, Comput. Phys. Commun. **153**, 275 (2003) [hep-ph/0301101].
- [9] W. Porod and F. Staub, Comput. Phys. Commun. **183**, 2458 (2012) [arXiv:1104.1573 [hep-ph]].
- [10] CMS Collaboration [CMS Collaboration], CMS-PAS-SUS-13-002.
- [11] W. Beenakker, R. Hopker, M. Spira and P. M. Zerwas, Nucl. Phys. B **492**, 51 (1997) [hep-ph/9610490].
- [12] M. Kramer, A. Kulesza, R. van der Leeuw, M. Mangano, S. Padhi, T. Plehn and X. Portell, arXiv:1206.2892 [hep-ph].
- [13] T. Sjostrand, S. Mrenna and P. Z. Skands, JHEP **0605**, 026 (2006) [hep-ph/0603175].
- [14] M. Papucci, J. T. Ruderman and A. Weiler, JHEP **1209** (2012) 035 [arXiv:1110.6926 [hep-ph]].
- [15] M. Papucci, K. Sakurai, A. Weiler and L. Zeune, Eur. Phys. J. C **74** (2014) 11, 3163 [arXiv:1402.0492 [hep-ph]].
- [16] J. S. Kim, K. Rolbiecki, K. Sakurai and J. Tattersall, JHEP **1412** (2014) 010 [arXiv:1406.0858 [hep-ph]].
- [17] M. Drees, H. Dreiner, D. Schmeier, J. Tattersall and J. S. Kim, Comput. Phys. Commun. **187** (2014) 227 [arXiv:1312.2591 [hep-ph]].
- [18] The ATLAS collaboration, ATLAS-CONF-2013-047, ATLAS-COM-CONF-2013-049.

- [19] G. Aad *et al.* [ATLAS Collaboration], JHEP **1409** (2014) 176 [arXiv:1405.7875 [hep-ex]].
- [20] G. Aad *et al.* [ATLAS Collaboration], JHEP **1310** (2013) 189 [arXiv:1308.2631 [hep-ex]].
- [21] [ATLAS Collaboration], ATLAS-CONF-2013-037, ATLAS-COM-CONF-2013-038.
- [22] The ATLAS collaboration, ATLAS-CONF-2013-062, ATLAS-COM-CONF-2013-039.
- [23] [ATLAS Collaboration], ATLAS-CONF-2013-007, ATLAS-COM-CONF-2013-006.
- [24] The ATLAS collaboration, ATLAS-CONF-2013-048, ATLAS-COM-CONF-2013-056.
- [25] G. Aad *et al.* [ATLAS Collaboration], JHEP **1406** (2014) 124 [arXiv:1403.4853 [hep-ex]].
- [26] G. Aad *et al.* [ATLAS Collaboration], JHEP **1406** (2014) 035 [arXiv:1404.2500 [hep-ex]].
- [27] V. Khachatryan *et al.* [CMS Collaboration], Eur. Phys. J. C **74** (2014) 9, 3036 [arXiv:1405.7570 [hep-ex]].
- [28] G. Aad *et al.* [ATLAS Collaboration], JHEP **1404** (2014) 169 [arXiv:1402.7029 [hep-ex]].
- [29] S. Chatrchyan *et al.* [CMS Collaboration], Eur. Phys. J. C **73** (2013) 12, 2677 [arXiv:1308.1586 [hep-ex]].
- [30] G. Aad *et al.* [ATLAS Collaboration], arXiv:1503.03290 [hep-ex].